SEBHA UNIVERSITY JOURNAL OF PURE & APPLIED SCIENCES VOL.XX NO. X 20XX
DOI: 10.51984/JOPAS.V24I1.3480

مجلة جامعة سبها للعلوم البحتة والتطبيقية
Sebha University Journal of Pure & Applied Sciences

Journal homepage: www.sebhau.edu.ly/journal/jopas

Mineral and Geochemical Approaches to Identify the Origin of Analcime in the Middle Carboniferous Dimbabah Formation, South-Western Libya

Alsedik Abousif*[a] Abdelmoniem Masoud[a] Moustfa Abdullah[a] Alsharef Albaghdady[b] Faraj Nasur[a] Mousi nizhah[c]

[a]Earth Sciences Department, Sebha University, Libya
[b]Earth Sciences Department, Libyan Academy, Libya
[c]Sirte Oil Company, Libya.

Keywords:
Murzuq Basin.
Dimbabah Formation.
Analcime bed.
X-ray diffraction.

ABSTRACT

The Dimbabah Formation, representing the final marine deposits in the Murzuq Basin, is widely exposed in various regions, including Al Awaynat, Wadi Irawan, Hasi Anjiwal, Bi'r Anzawa, Jabal Ati, the Anay region, and Hamadat Tanghirt. The presence of analcime within the Dimbabah Formation has raised questions about its origin, whether volcanic or lacustrine. Therefore, his study aimed to decipher the enigmatic occurrence of the analcime within the formation. X-ray diffraction (XRD) was used to identify the mineral composition of selected samples from representing two distinctive facies from the analcime beds. Also, X-ray flourecence (XRF) was used to investigate the bulk chemical composition. Scanning electron microscopy (SEM) and energy dispersive spectrometry (EDAX) was also used in this study to investigate the mineralogy and the chemistry of the selected samples. Based on these analyses and mineral associations, the analcime bed is interpreted as lacustrine deposits, suggesting the presence of an ancient playa lake or arid lagoon adjacent to the shoreline, potentially fed by one or more river tributaries. These evidences supported sedimentologically by the nature of analcime as oolitic and pseudo-oolitic, and the mud cracks within the facies. Althoght the volcanic ash was not observed in the sediments of the analcime beds, the volcanic materials contribution is not excluded since the eriontite and clinoptilolite zeolites are still recognized through the XRD analysis. Also, the geochemical data of the Dimbabah Formation's sample are nearly paired with igneous-type analcime.

الطرق المعدنية والجيوكيميائية للتعرف على أصل الانالسيم بتكوين دمبابة من الكربوني الاوسط في جنوب غرب ليبيا

الصديق ابوسيف[a]*، عبدالمنعم مسعود[a]، مصطفى عبدالله[a]، الشارف البغدادي[b]، فرج نصر[a]، موسى بن نزهة[c]

[a]قسم علوم الارض، جامعة سبها، ليبيا.
[b]قسم علوم الارض، الاكاديمية الليبية، ليبيا.
[c]شركة سرت للنفط، ليبيا.

الكلمات المفتاحية:
حوض مرزق.
تكوين ديمبابة.
طبقة الابالسيم.
حيود الاشعة السينية.

الملخص

صخور تكوين صخور دمبابة تمثل آخر الرواسب البحرية في حوض مرزق وتتكشف بمناطق شاسعة بما في ذلك العوينات، وادي إيروان، حاسي أنجيوال، بئر أنزوا، جبل عتي، منطقة اناي، وحمادة تانغرت. ولقد كان تواجد معدن الأنالسيم بتكوين دمبابة يثير عديد التساؤلات حول أصله، أهو ذو اصل بركاني أم رسوبي بحيري. لذلك تهدف الدراسة لفك لغز تواجد الانالسيم بهذا التكوين. تم استخدام حيود الأشعة السينية (XRD) لدراسة التركيب المعدني لعينات مختارة من طبقة الأنالسيم. كما تم استخدام فلورة الأشعة السينية (XRF) لفحص التركيب الكيميائي العام لها. وبالاضافة الى ذلك تم استخدام المجهر الماسح الإلكترونى (SEM) وتقنية التحليل الطيفي للطاقة (EDAX) في هذه الدراسة لدراسة المعادن

*Corresponding author.
E-mail addresses: als.abousif@sebhau.edu.ly, (A. Masoud) abd.masoud@sebhau.edu.ly, (M.Abdullah) mustafaabdullah72@yahoo.com, (A. Albaghdady) albaghdady@academy.edu.ly, (F. Nasur) far.nasour@sebhau.edu.*ly* ,(M. Nizhah) mosaissa86@gmail.com.
Article History : Received 18 August 24 - Received in revised form 23 March 25 - Accepted 02 May 25

والتركيب الكيميائي لها. بناء على هذه التحليلات والارتباطات المعدنية، فسر ت طبقة الأنالسيم كرواسب بحيرية، كبحيرة بلايا قديمة أو لاغون بمناطق جافة مجاورة للشاطئ، ربما تتغذى البحيرات من رافد نهري أو أكثر. تدعم هذه الأدلة رسوبيا طبيعة الأنالسيم كمعادن اوؤوليتية الشكل وشبه اوؤوليتية ، والشقوق الطينية كذلك لوحظت ضمن سحناتها. على الرغم من عدم ملاحظة الرماد البركاني في رواسب طبقة الأنالسيم، إلا أنه لا يمكن استبعاد مساهمة المواد البركانية نظرًا لظهور زيوليت اليريونتيت و الأكلينوبتيلوليت من خلال تحليل XRD. كما أن البيانات الجيوكيميائية لعينات تكوين دمبابة الانالسيمية قريبة من التطابق مع الأنالسيم من النوع البركاني.

1. Introduction

The Murzuq Basin, situated in southwest Libya between 21° -29° N and 10°-17° E, is one of many intracratonic basins on the North African platform and covers an area of about 350,000 km² (Fig. 1). The basin is bordered by the Qarqaf Uplift to the North, the Tihemboka Uplift to the west, and the Haruj and Tibesti Uplifts to the East, and its southern extension reaches into the Jadu Basin in Niger. The basin's present shape and structural relief bear the imprints of ancient tectonic events dating back to the Paleozoic and Mesozoic eras. Strata on the basin flanks dip towards the center, revealing a concentric pattern of Cambrian to Quaternary rock units. Despite undergoing successive erosive periods during phases of uplift and erosion, the central part of the Murzuq Basin boasts a maximum sedimentary thickness of approximately 4000 m, as reported by Davidson et al., 2000 [1].

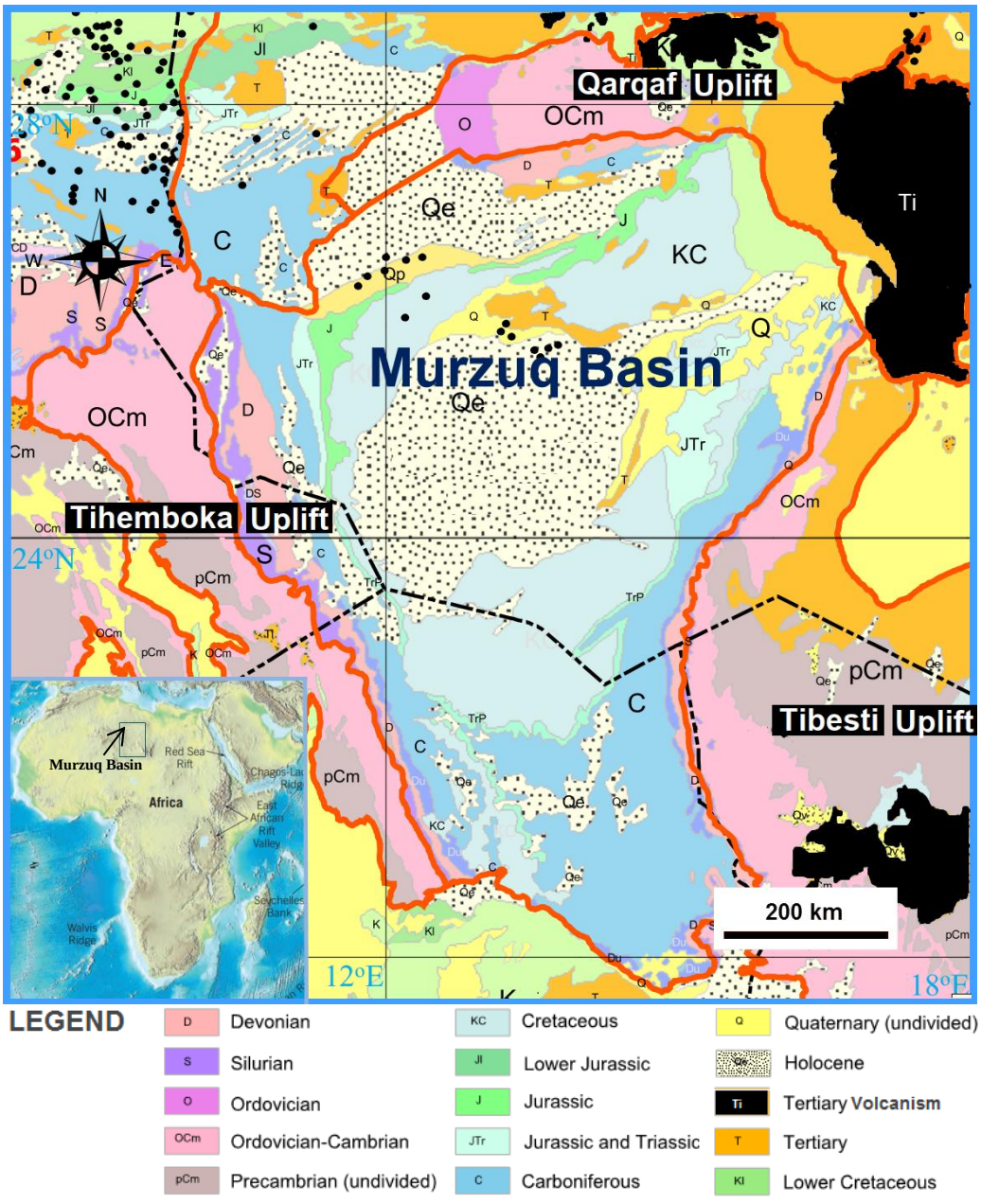

Fig. 1. Geological map of southren part of Libya shows the location and boundries of the Murzuq basin. Modified from Persits et al. (1997) [2].

The tectonic history of the Murzuq basin dates back to the late phases of the Pan-African Orogeny during the late Proterozoic to early Cambrian. Situated as a passive margin on the western side of Gondwana [3], multiple northwestern-southeastern trends of troughs and highs have formed, allowing various marine transgressions to inundate the early troughs. The current basin inherited two former

Pan-African troughs, namely the Murzuq-Jadu and the Dur al-Qussah-Uri troughs [4]. During the middle Devonian tectonism, the Tripoli-Tibesti uplift, which separated the two aforementioned troughs, collapsed, leading to the merging of the troughs in the Murzuq Basin. The final configuration of the basin was influenced by the Hercynian orogeny, which uplifted the Qarqaf uplift to block any subsequent marine transgressions.

The Dimbabah Formation is the final marine deposit in the Murzuq Basin and is visible in various areas such as Al Awaynat (Fig. 2), Wadi Irawan, Hasi Anjiwal, Bi'r Anzawa, Jabal Ati, the Anay region, and Hamada Tanghirt. Originally named by Lelubre (1946) without a designated type section, which was later assigned by Columb in 1960 [5, 6]. The formation stretches in a narrow northwest-southeast direction in the SW Murzuq Basin, with a thickness ranging from 25 m in the Anay area to the south to 110 m in the Bir Anzawa area to the north [7, 8] .

Stratigraphically, the Dimbabah Formation lies between the marine Assedjefar Formation from the Serpukhovian (Middle Carboniferous) and the continental Tiguentourine Formation from the Kasimovian (Late Carboniferous). Additionally, the formation rests above the older formation with a conformable surface and is separated from younger formations by an unconformity surface as in figure 2 [9, 10].

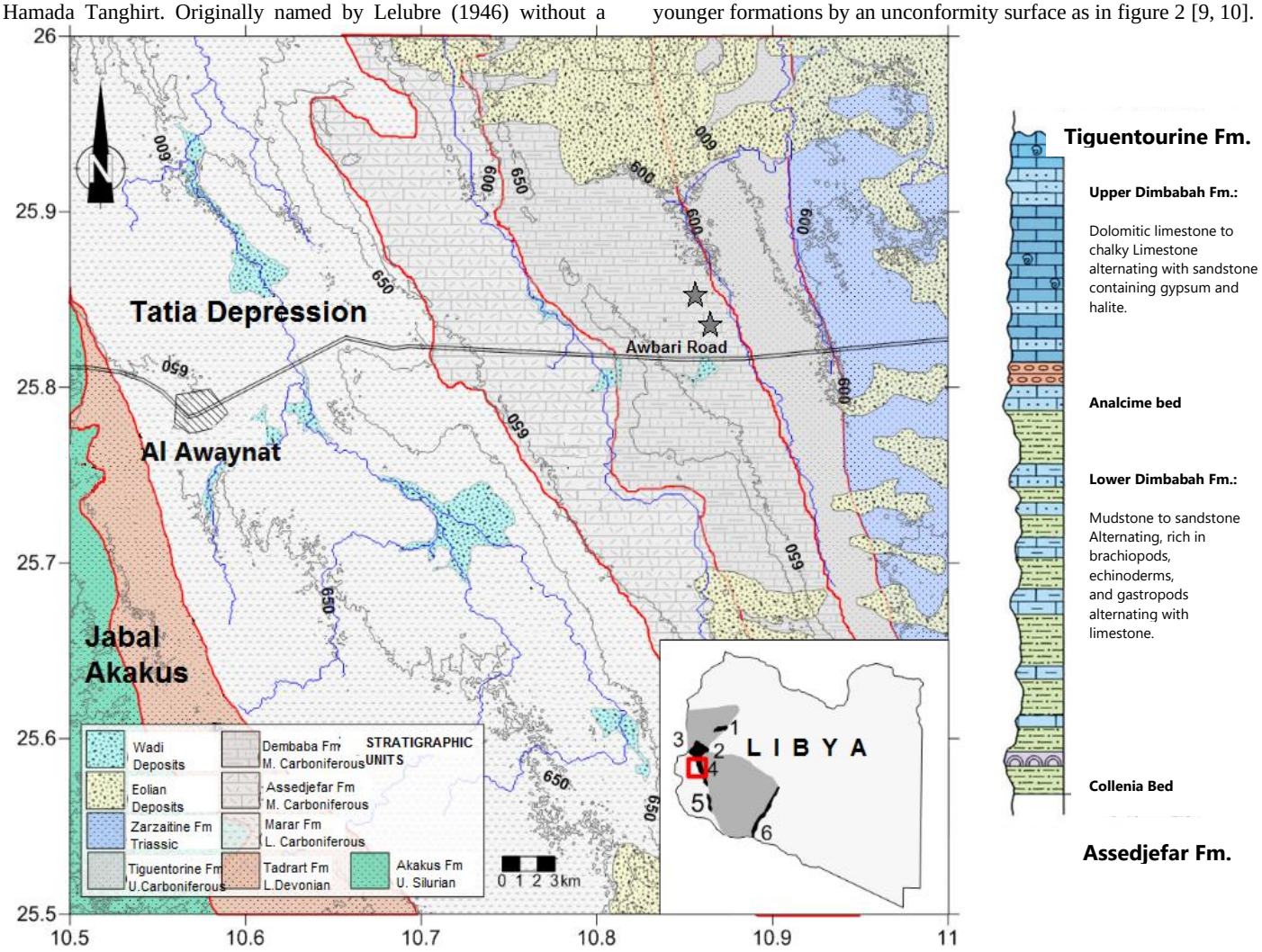

Fig. 2. A map illustrating the geological formations, geomorphological features, and sample collection points (marked with a star) within the study area. Locations: 1. Hamada Tanghirt (type section), 2. Hassi Anjiwal, 3. Bir Anzawa, 4. Al Awaynat (this study area and the coulmuner section after [10]), 5. Wadi Irawan, 6. Anay, 7. Jebel Ati (the columnar section on the right ~ 50 m). The gray color indicates the presence of the Dimbabah formation beneath the surface.

The Dimbabah Formation is divided into two parts (Fig. 2). The lower part is 60 m thick of gypsiferous claystone intercalated with a thin-bedded silty and clayey limestone. The limestone contains a stromatolite band in its lower part called the Collenia bed. The upper section is about 25 m thick of dolomitic limestone and dolomite intercalating with silt and claystone and siltstone. The Dimbabah Formation is rich in different fossils such as echinoderms, gastropods, brachiopods, foraminifera, conodonts, and corals, indicating its age dates back to the Bashkirian for its lower part and the Muscovian for its upper part [11, 12]. As for the sedimentary environment, it is considered a deep marine graded to shallow in its upper part. A layer of oolitic sandstone within the formation is known as the analcime bed, characterized by abundant of analcime mineral. In the area studied east of Al Awaynat town, this layer can reach a maximum thickness of 30 m, and is distinguished by a high thorium content, with levels reaching 13.5 ppm [11, 12].

This study addresses questions regarding the presence of analcime mineral in the carbonate deposits of Dimbabah Formation. It clarifies whether the mineral has a volcanic ash origin or lacustrine origin as reported by Karakaya, et al. [13]. Additionally, it highlights the environmental conditions that may have accompanied the onset of the Hercynian tectonic orogeny, establishing the Dimbabah Formation as the final evidence of the marine transgression in the Murzuq Basin during the middle Carboniferous period.

2. Methodology

Several samples have been collected from the studied area (Eastern Al Awaynat; Fig. 2), representing various facies within the analcime bed. The first facies consists of red fine- to medium-grained sandstone. The analcime minerals appear as white spots, averaging between 0.2 and 0.5 mm in size. The other facies is reddish-yellow, fine- to medium-grained sandstone, also featuring distinctive analcime spots. Both facies are characterized by mud cracks and minor laminations. Five samples were crushed using a mechanical agate mortar and pestle, then

sieved to 10-50 micrometers with 325 mesh copper sieves. The crushed samples were sent to the Mineralogisch-Petrographisches Institute at the University of Hamburg for XRD analysis. Additionally, part of the same samples was sent to the mechanical analysis lab at Sebha University, Department of Chemistry, for XRF analysis. Initially, X-ray diffraction (XRD) analysis was employed to determine the mineral composition of selected samples from the analcime bed. X-ray fluorescence was also utilized to investigate the bulk chemical composition of samples representing different facies. Furthermore, scanning electron microscopy (SEM) and energy dispersive spectrometry (EDAX) were employed to examine the analcime mineral and ascertain its chemical composition.

3. Results

3.1 Mineral composition

X-ray diffraction and SEM analysis provide a broad understanding of the mineral composition of very fine silt and clay grains, which are challenging to differentiate using traditional methods like the petrography. Samples from the analcime bed exhibit a similar pattern despite variations in grain size. Fig. 3 illustrates mineral peaks in the samples up to an angle of (2Θ) 40°, with some weaker peaks extending to 70°. The presence of higher angle peaks could be attributed to overlapping stronger peaks from other minerals. Key peaks for quartz, clinoptilolite, erionite, goethite, hematite, nontronite, and analcime are overlapped between 25° and 27°. Based on this study, it can be concluded that identified minerals are categorized according to their abundance, as detailed below:

Analcime ($Al_{1.8}H_{1.8}Na_{1.7}O_{14}Si_{4.1}$)

The presence of analcime mineral is the primary focus of this research. It has been confirmed in all examined samples through XRD and SEM analysis, particularly in both ANY and ANR samples. Fig. 3 illustrates the initial detection of analcime at a 15° angle, with the most significant peaks visible at 18° angles as depicted in Figure 3. Comparing our findings to those of Gatta, et al. [14], we estimate the presence of analcime in the samples to be approximately 88.2%, and the analcime mineral content in the ANR1 sample was approximated around 42.3% (Table 1).

Quartz (SiO_2)

The first appearing peak of quartz was detected at a 21° angle, and the highest reflectance was at 26°, as shown in Fig. 3. Quartz is a prevalent mineral in sandstone, even after the crushing process due to its high hardness. It is possible that the mineral content is higher than indicated by the matching program, estimated at around 29.4%, considering the qualitative and semi-quantitative nature of the XRD method. Quartz was identified in all samples analyzed, with samples ANY and ANR exhibiting higher quartz ratios. Following the calibration method introduced by Gualtieri [15], we estimate that the presence of quartz in the samples is approximately 87.7% accurate. Further coefficients can be found in Table 1.

Clinoptilolite-Na ($Al_{1.6}H_{30}Na_{2.06}O_{47.56}Si_{16.4}$)

The clinoptilolite-Na recognized significantly with a figure of merit of more than 54%. The peaks were weak, and more than 140 matched peaks were detected of 290 peaks of the Alberti [16] sample. The semi-quantitative analysis obtained from the XRD analysis showed that the percentage of the clinoptilolite was 21% (Table 1).

Dolomite ($Ca_{0.5}Mg_{0.5}CO_3$)

Dolomite significantly appears at a 2Θ angle of 31°, and sometimes it is overlapped by other peaks, like at 24° (Table 1 and Fig. 3). The percentage of the mineral in the sample was about 4%, and the figure of merit was 65% as it compared to Antao, et al.'s [17] experiment. Under these circumstances it is more accurate than calcite in the sample, but it is not a primary mineral as that for quartz and analcime.

Erionite-Ca ($Al_{3.954}Ca_{1.22}H_{72.096}K_6Mg_{0.26}O_{49.2}Si_{14.046}$)

With a lower peak appearance than the upper mentioned zeolite mineral, erionite was recognized too. The percentage was 1.5% and the FoM was 52.3% as compared to Gualtieri, et al. [18] sample.

Nontronite ($Fe_2O_6Si_2$)

According to Table 1 and the XRD plot depicted in Fig. 3, nontronite mineral (smectite clay) was detected at ANR sample at a confirmation rate exceeding 49%. Its presence in the sample was accounted for approximately 0.8%, semi-quantitatively. The identification was made possible by comparing it with the sample obtained from Garfield, Washington [19].

Table 1: Shows the XRD parameters for the analcime layer samples of the most important minerals that could be matched using the Match™ matching program.

	Analcime	**Quartz**	**Clinoptilolite-Na**	**Dolomite**	**Erionite-Ca**	**Nontronite**	**Calcite**	**Proto-Hematite**	**Goethite**
Composition	$Al_{1.8}H_{1.8}Na_{1.7}O_{14}Si_{4.1}$	SiO_2	$Al_{1.6}H_{30}Na_{2.06}O_{47.56}Si_{16.4}$	$Ca_{0.5}Mg_{0.5}CO_3$	$Al_{3.954}Ca_{1.22}H_{72.096}K_6Mg_{0.26}O_{49.2}Si_{14.046}$	Fe H O6 Si_2	$CaCO_3$	$Fe_{1.9}H_{0.06}O_3$	**$FeHO_2$**
Percentage	42.3%	29.4%	21.7%	4%	1.5 %	0.8%	0.3%	<0.1%	**<0.1 %**
Figure of merit	88.2%	87.7%	54.6%	65.33%	52.33%	49.16%	40.65%	68.11%	**60.6%**
Number of peaks	71	35	295	53	445	257	30	34	**86**
Matched peaks	35	18	143	16	124	66	7	14	**33**
Crystal system	Cubic	Trigonal (hexagonal axes)	Monoclinic	Trigonal (hexagonal axes)	Hexagonal	Monoclinic	Rhombohedral	Trigonal (hexagonal axes)	**Orthorhombic**
Density	2.22 g/cm³	2.64 g/cm³	2.11 g/cm³	2.838 g/cm³	2.282 g/cm³	2.99 g/cm³	4.03 g/cm3	5.21 g/cm³	**3.31 g/cm³**

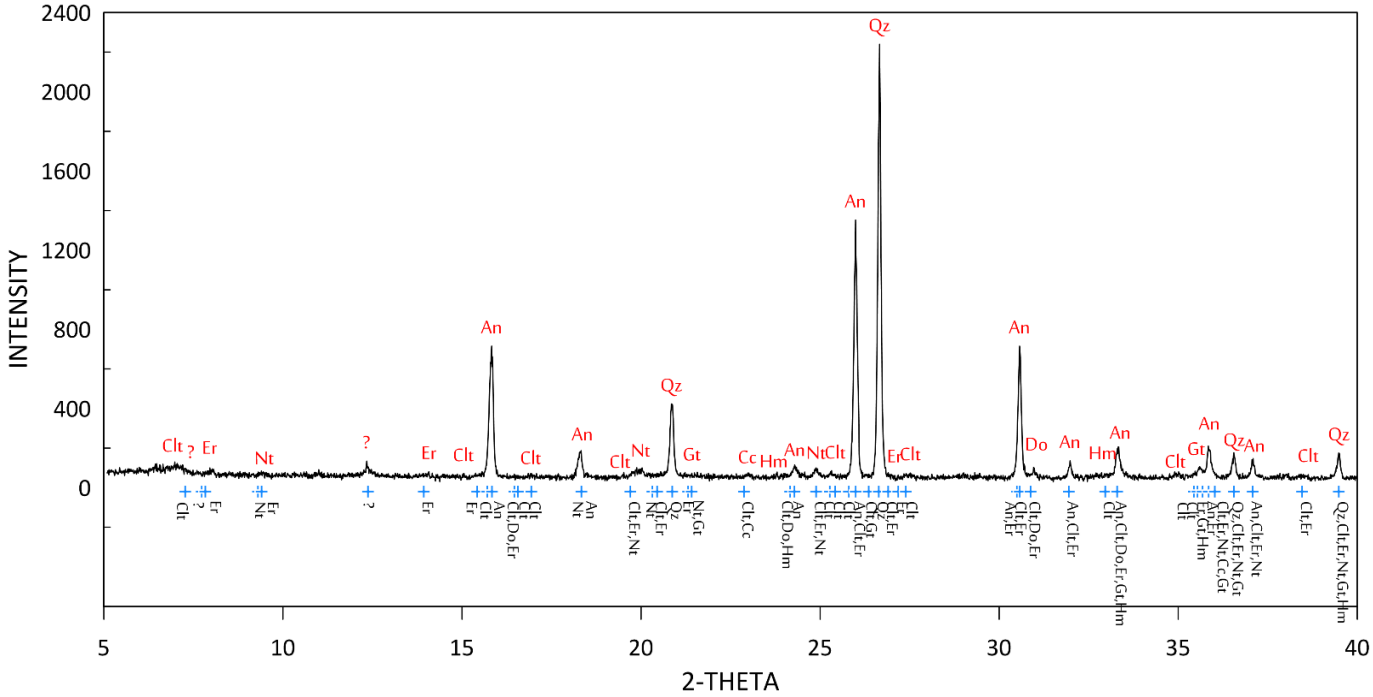

Fig. 3. X-ray diffraction pattern of samples ANR1 sample. Minerals shown include nontronite Nt, analcime An, quartz Qz, hematite Hm, goethite Gt, dolomite Do, eriontite Er, and clinoptilolite Clt. The (+) sign at the bottom indicates the 2-theta possible position of the overlapped mineral peaks.

Calcite ($CaCO_3$)

Although the semi-quantitative significant percentage of calcite in the sample, it showed very weakly developed peaks and sometimes overlapped by other strong mineral peaks like at 36° (Table 1 and Fig. 3). Calcite and the other carbonate minerals do not show up by the fizz test of the hand specimen, but it represents a significant comparison to the ideal calcite diffraction given by Wyckoff [20]

Goethite ($FeHO_2$)

According to Fig. 3, the presence of goethite mineral was observed in some of the samples studied. Our estimation of the verification degree of the goethite mineral's presence is approximately 60%, based on the same sample analyzed by Nagai, et al. [21]. The goethite's peaks are weakly developed, as well as in the other ferric oxides, and its percentage in the sample is considered <0.1 (Table 1).

Proto-Hematite ($Fe_{1.9}H_{0.06}O_3$)

In Fig. 3, hematite mineral was observed in all samples analyzed, playing a significant role in each one. It is easily recognizable by its distinct reddish-brown color in the hand specimen. The presence of hematite was confirmed by a 68% match to the samples studied by Gualtieri and Venturelli [22]. Although the higher FoM of the mineral, its peak and percentage still weak, in either its semi-crystallized form of hematite or its nature in the sample as a cement or grain-coating (Table 1).

3.2 Bulk Chemical Composition

The table represents the chemical composition of analcime-rich sandstone with two distinct facies: yellow (ANY) and red (ANR). Each facies is further divided into samples denoted as ANY1, ANY2, and ANY3 for the yellow facies, and ANR2, ANR3 for the red facies. The composition is quantified in terms of various oxides, each presented as a percentage of the total composition. The yellow facies is characterized by higher SiO_2 and Na_2O contents, while the red facies is enriched in Fe_2O_3 and TiO_2, reflecting the distinctive mineralogical and geochemical environments of these sandstone facies. The yellow facies samples (ANY1, ANY2, and ANY3) show a higher SiO_2 content, ranging from 64.61% to 72.8%, indicating a significant quartz presence. The red facies samples (ANR2, ANR3) have slightly lower SiO_2 content, ranging from 65.9% to 67.1%. Al2O3 content is relatively consistent across both facies, with the yellow facies ranging from 12.7% to 14.1% and the red facies ranging from 12.5% to 13.1%. The yellow facies exhibits a higher Na_2O content, especially in ANY1 (9.95%), compared to the red facies, which has significantly lower Na_2O values (2.24% to 3.10%). The red facies is notably richer in Fe_2O_3, with values of 12.8% and 14.2%, compared to the yellow facies, which ranges from 5.11% to 8.47%. MgO content is generally low across all samples, with the yellow facies ranging from 0.737% to 2.78% and the red facies showing slightly more consistent values around 0.957%. Both facies show variable CaO content, with the yellow facies ranging from 1.63% to 3.02% and the red facies from 1.39% to 1.69%. The content of TiO_2 is somewhat higher in the red facies (1.72% to 1.8%) compared to the yellow facies (1.05% to 2.11%). K_2O is present in minor amounts, with slightly higher values in the red facies (0.487% to 0.595%) compared to the yellow facies (0.227% to 0.43%). MnO is also present in trace amounts, with the yellow facies having values from 0.0352% to 0.0869% and the red facies from 0.0919% to 0.102%.

Table 2: Illustrates the chemical composition of the abundant elements in the sample of the analcime layer with a dumbbell structure.

Oxide	• NY1	A	• NY2	A	• NY3	A	• NR3	• NR2	A
SiO_2	• 4.61	6	• 2.8	7	• 8.7	6	• 5.9	• 7.1	6
Al_2O_3	• 4.1	1	• 4	1	• 2.7	1	• 2.5	• 3.1	1
Na_2O	• .95	9	• .2	3	• .7	4	• .1	• .24	2
Fe_2O_3	• .11	5	• .97	5	• .47	8	• 4.2	• 2.8	1
MgO	• .78	2	• .938	0	• .737	0	• .957	• .957	0
CaO	• .96	1	• .63	1	• .02	3	• .69	• .39	1
TiO_2	• .05	1	• .94	1	• .11	2	• .8	• .72	1
K_2O	• .227	0	• .43	0	• .3	0	• .487	• .595	0
MnO	• .0352	0	• .0668	0	• .0869	0	• .102	• .0919	0

3.3 Scanning electron microscopy- Energy dispersive spectrometry SEM-EDAX

The SEM analysis microphotographs revealed grains with a size of approximately 0.5 mm, surrounded by a matrix of bright, egg-shaped, possibly hematitic cement and flaky clays, likely smectite, morphologically (Fig. 4A, C, and D). Brighter grains, believed to have a higher atomic number, were detected around the AZ 047 D 701 spot area (Fig. 4C). Furthermore, the EDAX microprobe indicated the presence of iron in the bright areas within a range of 13.9 to 19.1 wt%. The 701 area represents a cluster of two different minerals, not one, based on the carbon-iron content and silicon-oxygen content. These

minerals are siderite and nontronite, with a tendency to lean towards siderite or a nontronite with a higher Fe content. The siderite either contained a nontronite inclusion within it or was coated by it. The AZ 047 D 697 spot showcased an exposed crystal of analcime (not coated with the matrix or cement; Fig. 4A). The composition included small traces of Mg, Fe, Ca, and Ti as impurities or substitutions but still aligned with the proportional composition of analcime.

4. Discussion

4.1 Analcime Occurrence

Analcime is a zeolite mineral found in association with other minerals and embedded in various rock types. Analcime mineral are categorized under two main origin categories, including the volcanic- and lacustrine- origin analcime [13]. In igneous rocks, it serves as a secondary filler in basalt cavities (the Cyclopean Islands in Sicily, Italy), decomposed volcanic ash fragments containing clinoptilolite and/or phillipsite zeolites in lake sediments such as the Wikieup Formation in Arizona, USA [23], or is an essential mineral of volcanic clastic sediments altered by metamorphism or hydrothermal solutions [23-25]. Volcanic analcime is often found accompanying plagioclase, biotite, quartz, amphibole, and various metal oxides, as well as other zeolite minerals like chabazite, erionite, and clinoptilolite [13].

Away from igneous activities, analcime minerals are found along the edges of lakes or tidal flats that are both highly saline and alkaline. It may form pure analcime layers called analcimolite, and one of the most famous places of its presence is the Pogo Agie member of the Chugwater Formation in Wyoming, America [26]. Based on the literatures, the most famous sandy facies containing analcime minerals were reported from the lake sediments in Olduvai Gorge in Tanzania [27]. The lacustrine analcime minerals are associated with minerals such as calcite, quartz, limonite, fluorite, smectite, feldspar, and mica. According to [13], the analcime minerals were observed in soils in dry climates adjacent to alkaline lakes, as is the case in California, East Africa, India, and Russia [23]. Goethite, as an associated mineral, is found in lake deposits and salt marshes. The formation of the goethite mineral has been reported in ancient lakes with various small tributaries that supplied continental deposits to the lake. These continental deposits are often associated with iron oxidation conditions. Hematite is commonly found in oxidized sedimentary environments, often in the form of rust, particularly in zoned iron deposits like oolitic iron deposits.

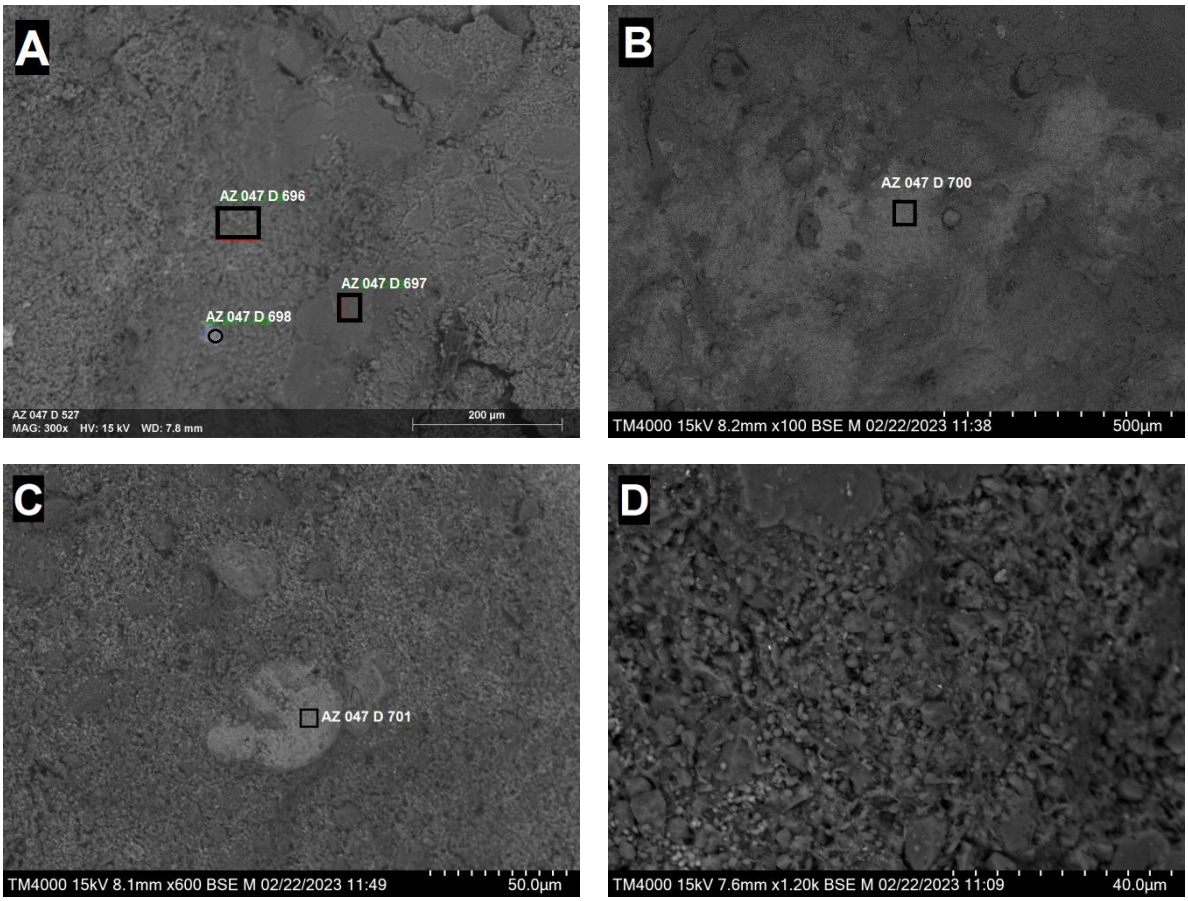

Fig. 4. SEM microphotograph of a sample collected from the analcime bed of the Dimbabah Formation showing the mineral phase and morphology of the matrix and the grains. The squares and the circle at A, B, and C show the area of the EDAX spectrum position in Table 3.

Table 3. EDAX microanalysis of the analcime samples shows in the major element concentrations in wt % at the spot area shown in Fig. 4.

Spectrum	C	O	Na	Mg	Al	Si	S	Cl	Ca	Ti	Fe	Ni
AZ 047 D 696	10.05	64.54	0.44	1.13	3.07	19.03			0.31	0.48	0.96	
AZ 047 D 697		58.91	1.12	1.39	4.75	32.13			0.41	0.53	0.75	
AZ 047 D 698		66.02	0.68	1.46	2.86	8.22			0.65	1	19.11	
AZ 047 D 700		58.56	2.21	0.59	3.08	17.2	0.98	0.79	1.61	0.66	14.32	
AZ 047 D 701	6.65	41.52			2.82	33.62			0.96	0.48	13.93	0.01
Mean	8.35	57.91	1.11	1.14	3.32	22.04	0.98	0.79	0.79	0.63	9.81	0.01
Sigma	2.4	9.74	0.78	0.4	0.81	10.72	0	0	0.52	0.22	8.43	0
Sigma Mean	1.08	4.36	0.35	0.18	0.36	4.79	0	0	0.23	0.1	3.77	0

According to Faure [28], analcime minerals are chemically formed by the decomposition of clastic albite mineral, clay minerals such as illite and montmorillonite, or from sodium-rich solutions or from post-decomposition processes of clinolitelite or volcanic materials. There are many examples of analcime minerals that have originated from the decomposition of montmorillonite in high salinity lakes such as Soda Lake in Kenya with complete absence of volcanic materials as reported by several workers such as [29] and [30].

In the study area, the analcime mineral's characteristics indicated the brackish lakes, sabkhahs, or playas origin in this case. The macrofacies of the analcime-host rocks show remarckable evidence of arid conditions through the mud cracks facies (Fig. 5). The analcime found here is oolitic and pseudo-oolitic, lacking any trapezoidal-shaped euhedral crystals. The presence of carbonate minerals was confirmed

in this study using XRD and SEM-EDAX analysis. Hematite and goethite are two other minerals found in these sediments. Nonetheless, XRD analysis can identify volcanic-type analcime minerals such as clinoptilolite and erionite. Analcime, according to various researchers, can form in an environment where brackish lake processes interact with volcanic ash carried to the region by air or water.

Fig. 5. Illustrates a distinct sedimentary facies within the analcime bed, featuring red and yellow sandy facies, as well as visible mud cracks.

4.2 Carboniferous Volcanic Activities

During the late Carboniferous period, the Pangaea supercontinent was formed, with significant volcanism accompanying the subduction of the Rheic and/or Proto-Tethys oceans, which separated the Gondwana and Laurasian continents. In the study area, the Sirte arch, which formed later during the Hercynian movement, eroded the Paleozoic rocks that capped the Sirte arch extensively. However, according to Guiraud, et al. [31], volcanic activity during the Bashkirian and Muscovian periods occurred about 600 kilometers from the study area region (Fig. 6).

4.3 Petrographical Aspects for the Origin of Analcime

Based on the field study and petrographic investigations, there is no evidence of any volcanic ash particles, nor did volcanic glass fragments occur within the studied samples from the study area. According to Karakaya et al., the volcanic analcime mineral is usually accompanied by a distinctive mineral company that differs from that of the lacustrine deposit. Among the volcanic analcime are amphibole, plagioclase, biotite, quartz, and zeolite minerals such as erionite, and clinoptilite. However, these above-mentioned minerals have shown up in the XRD investigations even with a good to moderate figure of merit.

The lake sedimentary origin of the analcime mineral is confirmed by the sedimentary nature as an oolitic analcime and the mud cracks. Also, the presence of a suitable mineral companion for lacustrine analcime was detected by the XRD and SEM. Among the minerals associated with it are smectite (nontronite), which was found with an accuracy of 49%. Nontronite mineral have been found in salty marine and lagoon environments. The presence of analcime mineral accompanied by a distinctive mineral company such as nontronite is reported from lagoon environments and has a sedimentary origin. The presence of sedimentary iron minerals is represented by hematite, which is formed in a high-energy oxidizing lake environment, as well as goethite, which is deposited in a non-stagnant lake environment with one or more tributaries that provide the oxidized environment in the ancient lake. The analcime mineral of the Dimbabah Formation differs from that studied in Turkey by the presence of iron oxide minerals (hematite and goethite) compared to the presence of feldspar and dolomite minerals in the sedimentary analcime studied by Karakaya *et al.*

This may be attributed to the hypothesis that the analcime mineral sedimentary origin with a significant contribution of volcanic input through the air and/or streams to a playa lake or coastal lagoons. Palaeogeographical maps prepared by Guiraud *et al.,* testify that the study area was submerged under shallow marine conditions. These conditions allowed the sedimentation of limestone deposits at the same time as the transitional ones that allowed the deposition of white sandstone near the beach at least.

4.4 Geochemical Aspects for the Origin of Analcime

Based on geochemical investigation conducted by Karakaya et al., there are variations in the chemical composition between the analcime inherited from volcanic origin compared to the sedimentary at several levels because the chemically stable elements are able to give an indication of the composition of its volcanic origin.

Sodium oxide, in particular, was richer in analcime of sedimentary origin compared to that occurs in mudstone almost are associated with volcanic activity such as zeolite tuff and lava deposits. The sodium oxide does not exceed 3.81% in the igneous-originated analcime, as shown in Fig. 7, with an average of 2.37%, while this number is higher in the sedimentary-originated analcime. Compared to our investigated samples of the Dimbabah Formation, they are almost similar to igneous-type analcime, and that could be applied to the Al_2O_3 and K_2O as well (Fig. 7).

In Karakaya et al. and Mao et al.' studies the alkaline oxides are different in both types of analcime, but the Earth alkaline oxides were significantly higher in the analcime associated with sedimentary rocks when compared to the analcime associated with igneous rocks. The same procedure has been applied to the samples of the Dimbabah Formation, which appear to be similar to those of the sedimentary type. The excessive increase in these oxides in the Anatolian samples is due to the fact that they contain a significant amount of carbonate minerals compared to the analcime bed in the Dimbabah Formation associated with the clastic sandstone. That could also be recognized by the low total alkali to total alkali earth ratio of sedimentary-type analcime as in Fig. 7. Again, that also showed the ratio of the studied sample is close to the igneous-type analcime.

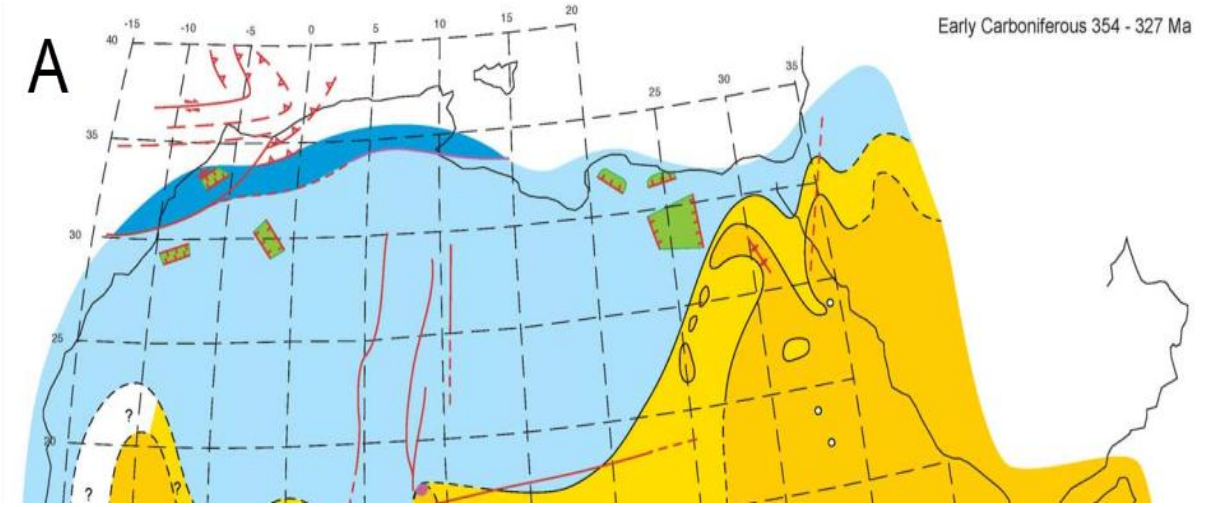

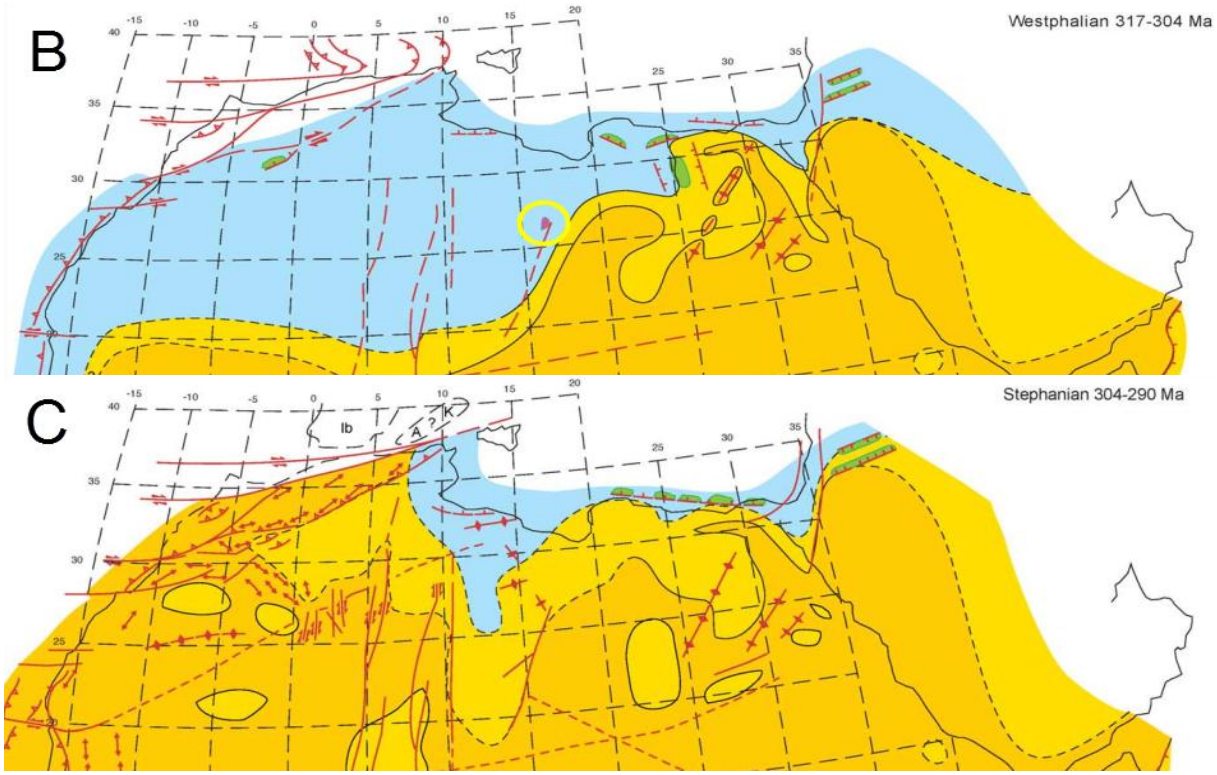

Fig. 6. Geographical maps of North Africa during the Lower Carboniferous (A), Bashkirian-Moscovian (B), and Upper Carboniferous (C) periods [31]. The potential volcanism in the Bashkirian and Moscovian is indicated by a circle and arrow in map B. Map key: (1) continental, exposed land; (2) continental basin; (3) platform; (4) slope and deep marine; (5) effusive magmatism; (6) fault; (7) normal fault; (8) active rift or subsident basin; (9) depocenter axis; (10) strike-slip fault; (11) anticline axis; (12) thrust; (13) active high; (14) oceanic ridge; (15) annular alkaline complex; (16) dyke.

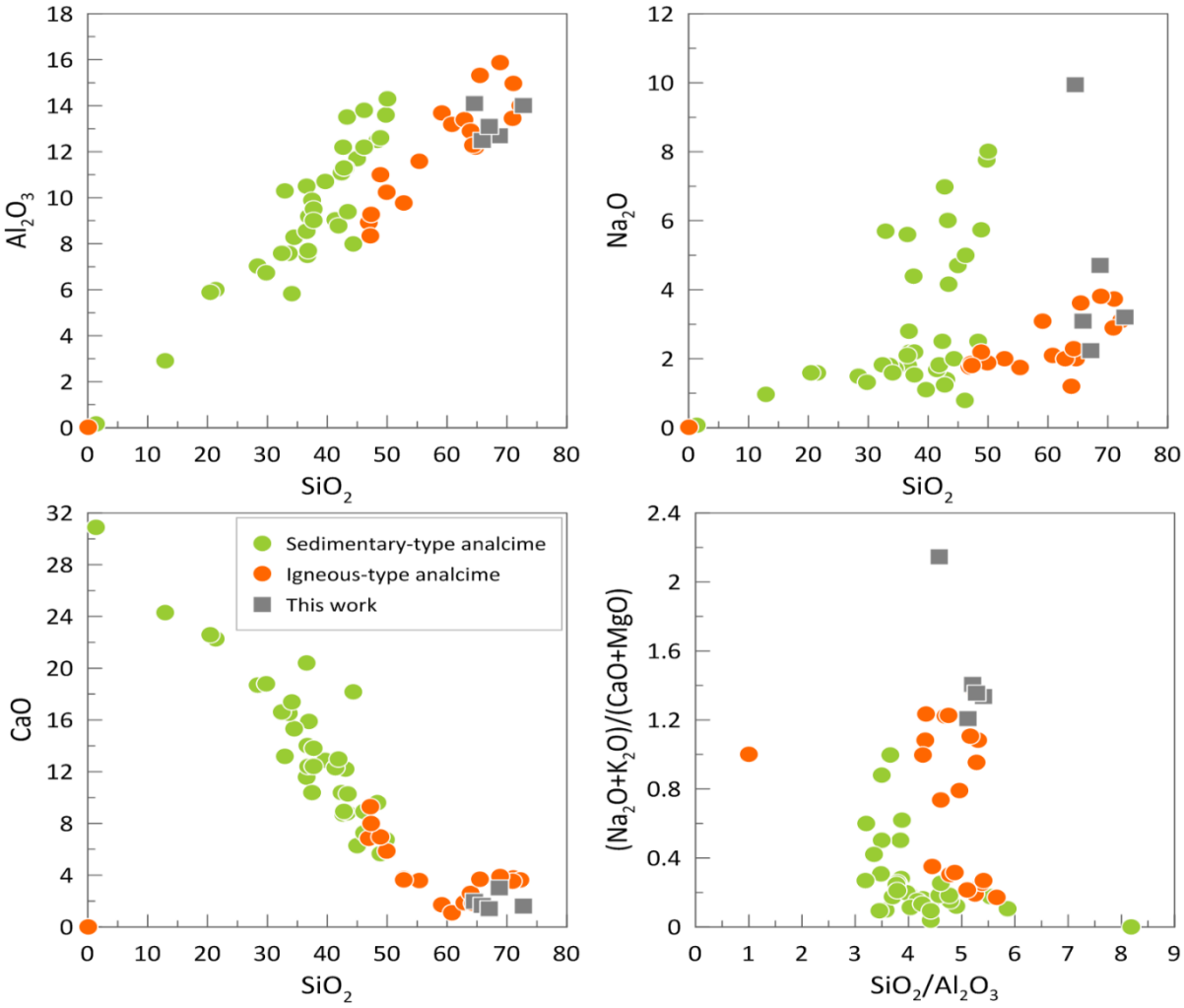

Fig. 7. Harker plot for Al_2O_3, Na_2O, and CaO against SiO_2 and the silica-alumina ratio against the total alkali-total alkali Earth ratio, showing the variation of the igneous-type analcime and sedimentary-type analcime of the studied Dimbabah formation's samples compared to the Karakaya et al., study.

5. Conclusion

In conclusion, the findings of this study contribute to a better understanding of the geological history and environmental conditions of the Murzuq Basin during the middle Carboniferous period. By clarifying the origin of analcime within the Dimbabah Formation, this research provides valuable insights into past environments and tectonic events in the region.

The presence of analcime within the Dimbabah Formation in the Murzuq Basin of southwestern Libya has been investigated using mineralogical and geochemical approaches. Through X-ray diffraction (XRD), X-ray fluorescence (XRF), and scanning electron microscope (SEM) analyses, it has been determined that the analcime bed in the Dimbabah Formation is of sedimentary origin in arid or semi-arid conditions of playa or lagoon adjacent to a shoreline fed by river tributaries with a significant volcanic material input to it. This conclusion is supported by the absence of volcanic ash in the sediments, but the presence of igneous-type minerals (clinoptilolite and erionite) supporting that influx. Therefore, additional samples from other regions such as Hamada Tanghirt, Hassi Anjiwal, Bir Anzawa, Wadi Irawan, Anay, or Jebel Ati may contain traces of volcanic materials, which could be recommended for further study. The oolitic nature, the presence of mud cracks, and sedimentary-type analcime-associated minerals (nontronite, dolomite, and iron oxide minerals) are absolutely refers to as an active sedimentary environment.

Furthermore, the geochemical composition of the analcime bed is characterized by high levels of aluminum oxide and low levels of sodium and calcium oxides. It's recommended to perform REE analysis to these samples to get more signature of the volcanic materials if there any. All of our samples were close to the igneous-type analcime of the other studies and supports the volcanic material influx, especially with a notice of nearby volcanic activity during the Middle-Late Carboniferous period that was associated with a great tectonic instability associated with the Pangea assembly.

6. Acknowledgment

We would like to express our gratitude to everyone who assisted us with this research, including Dr. Yvonne Milker from the Center for Earth System Research and Sustainability and Dr. Thomas Malcherek from the Mineralogisch-Petrographisches Institute at the University of Hamburg. Additionally, we wish to extend a special note of thanks to the Libyan Petroleum Institute for their contribution. Finally, we are deeply grateful to the anonymous individuals who will review this article.

7. References

[1] Davidson, L., Beswetherick, S., Craig, J., Eales, M., Fisher, A., Himmali, A., (2000), The Structure, Stratigraphy and Petroleum Geology of Murzuq Basin, Southwest Libya, in Geological Exploration in Murzuq Basin, Elsevier, Amsterdam, 295–320.

[2] Persits, F., Ahlbrandt, T. S., Tuttle, M. L., Charpentier, R. R., Brownfield, M. E., Takahashi, K. I., (1997), Maps showing geology, oil and gas fields and geological provinces of Africa, US Geological Survey, 2331-1258.

[3] Torsvik, T. H., Cocks, L. R. M., (2011), The Palaeozoic palaeogeography of central Gondwana, Geological Society, London, Special Publications, **357**, 137–166.

[4] Klitzsch, E., (1971), The structural development of parts of North Africa since Cambrian time, in First Symposium on the Geology of Libya, Gray, C., Ed., Faculty of Science, University of Libya, Tripoli, 253–262.

[5] Massa, D., Collomb, G., (1960), Observations nouvelles sur la region d'Aouinet Ouenine et du Djebel Fezzan (Libye), in Proceedings of the 21st International Geological Congress, Copenhagen, Vol. 12.

[6] Lelubre, M., (1946), Sur la Paléozoïque du Fezzan, C.R. Hebd. Seanc. Acad Sci., **222**, 1403–1404.

[7] Belhaj, F., (1996), Palaeozoic and Mesozoic stratigraphy of eastern Ghadamis and western Sirt basins, The Geology of Sirt Basin, **1**, 57–96.

[8] Wennekers, J., Wallace, F., Abugares, Y., (1996), The geology and hydrocarbons of the Sirt Basin: a synopsis, The Geology of Sirt Basin, 1, 3–56.

[9] Gundobin, G., (1985), Geological map of Libya 1:250,000, Sheet: Qararat al Marar, Explanatory Booklet, Industrial Research Centre, Tripoli.

[10] Röhlich, P., (1974), Geological map of Libya, 1:250,000. Sheet Al Bayda (NI 34–15), Explanatory Booklet, Industrial Research Centre, Tripoli.

[11] Berendeyev, V., (1985), Geological map of Libya 1:250,000 scale, Sheet Hamadat Tanghirt, NH32-16, Explanatory Booklet, Industrial Research Centre, Tripoli, p. 125.

[12] Vachard, D., Massa, D., (1984), The Carboniferous of Western Libya, in Biostratigraphy. International Congress on Carboniferous Stratigraphy and Geology, 165–174.

[13] Karakaya, N., Karakaya, M. C., Temel, A., (2013), Mineralogical and chemical properties and the origin of two types of analcime in SW Ankara, Turkey, Clays and Clay Minerals, 61, 231–257.

[14] Gatta, G. D., Nestola, F., Ballaran, T. B., (2006), Elastic behavior, phase transition, and pressure induced structural evolution of analcime, American Mineralogist, 91, 568–578.

[15] Gualtieri, A. F., (2000), Accuracy of XRPD QPA using the combined Rietveld–RIR method, Journal of Applied Crystallography, 33, 267–278.

[16] Alberti, A., (1975), The crystal structure of two clinoptilolite, unpublished.

[17] Antao, S. M., Mulder, W. H., Hassan, I., Crichton, W. A., Parise, J. B., (2004), Cation disorder in dolomite, $CaMg(CO_3)_2$, and its influence on the aragonite + magnesite ↔ dolomite reaction boundary, American Mineralogist, 89, 1142–1147.

[18] Gualtieri, A., Artioli, G., Passaglia, E., Bigi, S., Viani, A., Hanson, J., (1998), Crystal structure–crystal chemistry relationships in the zeolites erionite and offretite, American Mineralogist, 83, 590–606.

[19] Dainyak, L. G., Zviagina, B. B., Rusakov, V. S., Drits, V. A., (2006), Interpretation of the nontronite-dehydroxylate Mössbauer spectrum using EFG calculations, European Journal of Mineralogy, 18, 753–764.

[20] Wyckoff, R. W., (1920), The crystal structures of some carbonates of the calcite group, American Journal of Science, 50, 317–360.

[21] Nagai, T., Kagi, H., Yamanaka, T., (2003), Variation of hydrogen bonded O···O distances in goethite at high pressure, American Mineralogist, 88, 1423–1427.

[22] Gualtieri, A. F., Venturelli, P., (1999), In situ study of the goethite-hematite phase transformation by real time synchrotron powder diffraction, American Mineralogist, 84, 895–904.

[23] Deer, A., Howie, R., Wise, W., Zussman, J., (2004), Rock Forming Minerals. Volume 4B. Framework Silicates: Silica Minerals, Feldspathoids and the Zeolites, The Geological Society, London, UK.

[24] Bargar, K., Beeson, M., (1985), Hydrothermal alteration in research drill hole Y-3, Lower Geyser Basin, Yellowstone National Park, Wyoming, US Geological Survey Professional Paper.

[25] Utada, M., Ito, T., (1988), Promising geothermal resources in the Neogene volcanitectonic depressions along the volcanic front of northern Honshu, Japan, unpublished.

[26] High, L. R., Picard, M. D., (1965), Sedimentary petrology and origin of analcime-rich Pogo Agie Member, Chugwater (Triassic) Formation, west-central Wyoming, Journal of Sedimentary Research, **35**, 49–70.

[27] Fogle, K., (2021), Analysis of sediments cores from lake basin of Olduvai using X-ray diffraction, unpublished.

[28] Faure, G., (1998), Principles and Applications of Geochemistry, Upper Saddle River: Prentice Hall.

[29] Velde, B., (1985), Clay Minerals, Elsevier.

[30] Hay, R. L., Sheppard, R. A., (2001), Occurrence of zeolites in sedimentary rocks: An overview, Reviews in Mineralogy and Geochemistry, **45**, 217–234.

[31] Guiraud, R., Bosworth, W., Thierry, J., Delplanque, A., (2005), Phanerozoic geological evolution of Northern and Central Africa: an overview, Journal of African Earth Sciences, **43**, 83–143.

[32] Mao, Z., Fang, X., Yang, Y., Ye, C., Zhang, T., Zhang, W., Zan, J., (2020), Geochemical discrimination of the altered volcanic tuff from sediments in the Lunpola Basin, central Tibetan Plateau, Clay Minerals, **55**, 303–319.